A complete U-V-disparity study for stereovision based 3D driving environment analysis

Conference Paper · July 2005

DOI: 10.1109/3DIM.2005.6 · Source: IEEE Xplore

3 authors:

Zhencheng Hu
Kumamoto University
71 PUBLICATIONS **527** CITATIONS
SEE PROFILE

F. Lamosa
Omron, Kyoto
4 PUBLICATIONS **53** CITATIONS
SEE PROFILE

Keiichi Uchimura
Kumamoto University
127 PUBLICATIONS **704** CITATIONS
SEE PROFILE

A Complete U-V-Disparity Study for Stereovision Based 3D Driving Environment Analysis

Zhencheng Hu [†], Francisco Lamosa [‡] and Keiichi Uchimura [‡]
[†] *Department of Computer Science, Kumamoto University, Japan*
[‡] *Graduate School of Science and Technology, Kumamoto University, Japan*
hu@cs.kumamoto-u.ac.jp, frank@navi.cs.kumamoto-u.ac.jp, uchimura@cs.kumamoto-u.ac.jp

Abstract

Reliable understanding of the 3D driving environment is vital for obstacle detection and Adaptive Cruise Control (ACC) applications. Laser or millimeter wave radars have shown good performance in measuring relative speed and distance in a highway driving environment. However the accuracy of these systems decreases in an urban traffic environment as more confusion occurs due to factors such as parked vehicles, guardrails, poles and motorcycles. A stereovision based sensing system provides an effective supplement to radar-based road scene analysis with its much wider field of view and more accurate lateral information. This paper presents an efficient solution using a stereovision based road scene analysis algorithm which employs the "U-V-disparity" concept. This concept is used to classify a 3D road scene into relative surface planes and characterize the features of road pavement surfaces, roadside structures and obstacles. Real-time implementation of the disparity map calculation and the "U-V-disparity" classification is also presented.

1. Introduction

Adaptive Cruise Control (ACC) and collision safe technologies are two of the most active research fields in ITS in order to provide effective driver assistance and protection. In a typical ACC scenario, a safe distance between vehicles is automatically maintained by the system while minimizing the difference between desired and the actual velocity. At times of danger, alarm and braking assistance will be trigged, or the seat belt is tightened as a function of the distance between two vehicles.

A driving environment analysis system typically extracts the road surface, detects obstacles, and computes the position of obstacles relative to the vehicle by using range information. Conventionally, active sensing systems like laser radars or millimeter wave radars have been shown to provide good performance in ACC applications. Laser radar measures the distance between two vehicles by irradiating the scene ahead of the vehicle with an infrared laser beam and measuring the time lag of the received catoptrical light. Although a laser radar system provides high accuracy measurements at a relatively low cost, it is very sensitive to bad weather, such as rain, fog, and snow and will interfere with the laser emitted from other vehicles. Millimeter wave radar measures distance by detecting the reflected waves. Since it provides sufficient accuracy even under bad weather conditions, millimeter wave radars are widely adopted in the ACC and collision safety applications of recent years.

However, some vital weaknesses exist in these radar sensors. Generally, radar has a very narrow field of view (less than 15 degrees, even for the expensive mechanical scanning radar systems) and lower accuracy in lateral directions. This means that a radar system can hardly "see" a cutting-in or passing-by vehicle from neighboring lanes unless the vehicle is far ahead (most off-the-shelf radar systems have blind range of 15 to 20 meters in neighboring lanes). Moreover, since no clues exist about road shape information for a radar system, it cannot distinguish between an in-path obstacle and out-of-path obstacle, especially if the obstacle is located in incoming curves.

Stereovision sensors can compensate for all these shortcomings of radar systems. Stereo analysis is the process of measuring range to an object by comparing the object projection on two or more images. Until recently, real-time stereo analysis could only be implemented in large custom hardware arrays. But recent advances in computational power and algorithms have made it possible for general-purpose personal computers to perform real-time stereo processing.

In the ITS field, many approaches have been proposed for the analysis of the driving environment based on stereovision technology [1][2][3]. Compared to radar systems, stereovision sensor has the advantages of a wide Field Of View (FOV), excellent lateral accuracy and relative low cost. The passive nature of stereovision sensor implies that it is relative free of signal interference

Proceedings of the Fifth International Conference on 3-D Digital Imaging and Modeling (3DIM'05)
1550-6185/05 $20.00 © 2005 **IEEE**

in the presence of other sensors. Further, it can provide both scene intensity and depth information (2.5-D). However, like other optical sensors, stereovision sensors are sensitive to poor weather and illumination conditions. It also suffers from the high computational cost of disparity map calculation, 3D scene reconstruction and analysis, which has greatly limited its application in solving real-world problem.

In this paper, we present an efficient solution of fast stereovision based road scene analysis algorithm, which employs the "U-V-disparity" concept to classify 3D road scene into relative surface planes and characterize the features of road pavement surfaces, roadside structures, and obstacles. Real-time implementation of disparity map calculation and "U-V-disparity" classification is also presented.

The paper is organized as follows: Section 2 quickly reviews previous work in stereo-based road environment analysis. "U-V-disparity" concept as well as features of different surface planes are described in Section 3. Section 4 shows implementation details and experimental results.

2. Previous work

A typical urban traffic scenario is shown in Fig. 1. Automotive engineers are facing the following challenges in analysing the 3D driving environment: 1) Detecting road surfaces and lane areas; 2) Recognizing obstacles above road surfaces, measuring their sizes and 3D models; 3) Measuring the relative distances between vehicle and obstacles; 4) Recognizing roadside structures like guardrails, lamp poles, over-pass bridges, etc. which are not obstacles but may be easily confused as such.

Optical flow forms the basis of vision-based 3D scene analysis and obstacle detection [4][5][6]. Most optical flow algorithms assume that the only motion between the camera and the environment is translation, which may not be true in most driving situations.

Fig.1. A typical urban driving scenario

Stereovision is also widely used in scene analysis [7]-[10]. Stereo analysis is the process of measuring range to an object by comparing the object projection on two or more images. To properly extract obstacles from the scene, it is necessary to separate the image features belonging to the road surface from those belonging to obstacle candidates. Most of the algorithms will employ a clustering method, applied successively, to merge sparse disparity pixels into separate obstacle candidates, making use of the constraint of disparity continuity.)

Luong and Koller [1] used the term “Helmholtz shear” to describe a simplified algorithm that extracts the obstacle candidates located above the road surface. Bertozzi [8] combines symmetry detection and stereo matching to extract vehicles in front and estimate their distance. Talukder [9] suggested a pre-set maximum and minimum distance between points belonging to a same obstacle, as well as a sufficiently high angle with the ground plane for all lines connecting both points. However, due to vehicle suspensions and uneven road surfaces, those algorithms are not tolerant enough to separate obstacle candidates from road surfaces. In addition, clustering the sparse disparity pixels into separate obstacle candidates is very time consuming as well as having limited accuracy. Some obstacles are simply removed due to the small number of detected disparity pixels or the limited dimension in depth.

Labayrade [10] proposed the “V-disparity” concept aimed at simplifying the process of separating obstacles from road surfaces, where “V” corresponds to the vertical coordinate in the (u, v) image coordinate system. In the “V-disparity” domain, the longitudinal profile of the road surface plane can be described as a piecewise linear curve, and obstacles in the vertical plane will be projected as a vertical line. Therefore extraction of 3D road surface and obstacles will be simplified as 2D linear extraction.

"V-disparity" is mainly used to extract surface planes which are perpendicular to the vertical plane of the stereo rig, like road surface plane and vehicle front surfaces. However in an uncontrolled driving environment, most obstacle surface planes do not satisfy the rule of “V-disparity”. For example, vehicle side surfaces, guardrails, roadside or overpass structure and many other surface planes cannot be projected as a simple linear curve on the "V-disparity" plane.

In this paper, we extend Labayrade’s work to a more general case for driving environment analysis. We have proposed an "U-V-disparity" concept to classify the 3D road scene into relative surface planes and characterize the features of road pavement surfaces, roadside structures, and obstacles. Real-time implementation of disparity map calculation and "U-V-disparity" classification algorithms are also presented.

Proceedings of the Fifth International Conference on 3-D Digital Imaging and Modeling (3DIM’05)
1550-6185/05 $20.00 © 2005 **IEEE**

3. The geometrical model of U-V-disparity

3.1. Basic principles of stereovision

The epipolar constraint states that a point of a 3D scene is projected on segments of corresponding epipolar lines. Therefore corresponding pixel matching between left and right cameras becomes an inherently 1D search problem. Two corresponding points determine the basic relation for disparity in stereo, which has a simple expression for coplanar cameras:

$$d = x_l - x_r = f\frac{b}{Z} \tag{1}$$

where d is disparity, x_l and x_r are horizontal coordinates of corresponding pixels on left and right images, f is camera focal, b is baseline distance and Z is depth. Fig.2 shows a general stereo camera set-up.

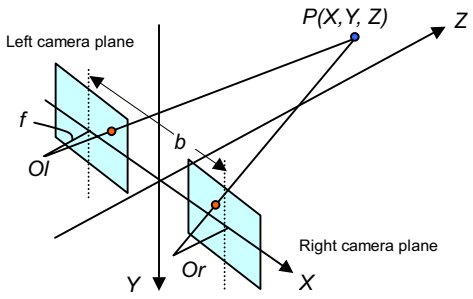

Fig.2. A general view of stereo camera set-up

3.2. Domain of U-V-disparity

We assume that the stereo rig mounted on the vehicle has two coplanar cameras with the same intrinsic parameters and their horizontal co-axis is parallel to the road surface (see Fig.3), where the pitch angle to the ground plane is θ. To simplify the problem, we put the origin of World Coordinate System WCS (X_w, Y_w, Z_w) to the centre of the origins of two stereo Camera Coordinate Systems LCCS (X_l, Y_l, Z_l) and RCCS (X_r, Y_r, Z_r). The optical axis of the WCS is parallel to the ground plane and indicates the vehicle's direction of motion.

In the camera coordinate system, the position of a point in the image plane is given by its coordinates (u, v). The image coordinates of the projection of the optical centre will be denoted by (u_0, v_0), assumed to be at the centre of the image.

Based on Fig.3, the transformation from WCS to CCS is achieved by the combination of a vector translation of $\pm b/2$, and a rotation around X-axis by an angle of $-\theta$. Let T_l and T_r denote the translation matrices, R_l and R_r the rotation matrices from WCS to LCCS and RCCS respectively. The transformation matrices in homogeneous coordinates are therefore:

$$D_{l,r} = R_{l,r}T_{l,r} = \begin{bmatrix} 1 & 0 & 0 & \pm\frac{b}{2} \\ 0 & \cos\theta & -\sin\theta & 0 \\ 0 & \sin\theta & \cos\theta & 0 \\ 0 & 0 & 0 & 1 \end{bmatrix} \tag{2}$$

With the assumption of camera's aspect ratio equals 1.0 and the focal lengths are f for both left and right stereo cameras, the perspective projection matrix is expressed as follows:

$$P = \begin{bmatrix} f & 0 & u_0 & 0 \\ 0 & f & v_0 & 0 \\ 0 & 0 & 1 & 0 \end{bmatrix} \tag{3}$$

Therefore, we obtain the transformation between the WCS homogeneous coordinates $(X_w, Y_w, Z_w, 1)^T$ and the image coordinate $(u, v, 1)^T$:

$$\lambda\begin{bmatrix} u \\ v \\ 1 \end{bmatrix} = PD_{l,r}\begin{bmatrix} X_w \\ Y_w \\ Z_w \\ 1 \end{bmatrix} = M_{l,r}\begin{bmatrix} X_w \\ Y_w \\ Z_w \\ 1 \end{bmatrix} \tag{4}$$

where $M_{l,r}$ is the transformation matrix.

$$M_{l,r} = \begin{bmatrix} f & u_0\sin\theta & u_0\cos\theta & \pm b/2 \\ 0 & f\cos\theta + v_0\sin\theta & -f\sin\theta + v_0\cos\theta & 0 \\ 0 & \sin\theta & \cos\theta & 0 \end{bmatrix} \tag{5}$$

From equation (4) and (5), we can simply calculate the camera's image coordinates (u_l, v):

$$\begin{cases} u_{l,r} = u_0 + f\dfrac{X_w \pm b/2}{Y_w\sin\theta + Z_w\cos\theta} \\ v = v_0 + f\dfrac{Y_w\cos\theta - Z_w\sin\theta}{Y_w\sin\theta + Z_w\cos\theta} \end{cases} \tag{6}$$

To simplify equation (6), we denote a new set of image coordinates (U, V) with respect to the camera optical centre:

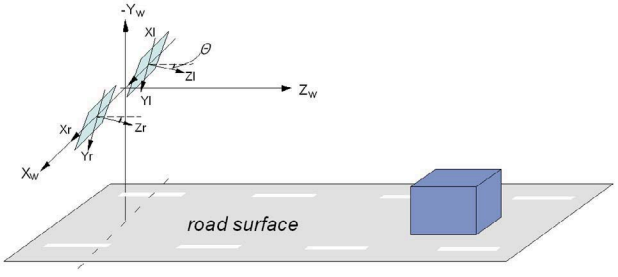

Fig.3. Relationship between the stereo coordinate system and the world coordinate system

$$\begin{cases} U_{l,r} = u_{l,r} - u_0 = f \dfrac{X_w \pm b/2}{Y_w \sin\theta + Z_w \cos\theta} \\ V = v - v_0 = f \dfrac{Y_w \cos\theta - Z_w \sin\theta}{Y_w \sin\theta + Z_w \cos\theta} \end{cases} \quad (7)$$

Disparity Δ can also be deducted from equation (7):

$$\Delta = u_l - u_r = f \frac{b}{Y_w \sin\theta + Z_w \cos\theta} \quad (8)$$

Equations (7) and (8) describe the basic relationship between image coordinates (U,V) and disparity Δ for a general coplanar stereo rig. This relationship can be also rewritten as the following set of simple expressions:

$$\begin{cases} U = \Phi(X_w, \Delta) \\ V = \Psi(Z_w, \Delta) \end{cases} \quad (9)$$

3.3. Various 3D planes projection in U-V-disparity

In Labayrade's work, three types of planes have been discussed with respect to the V-disparity concept: planes horizontal, vertical, or oblique relative to the stereo rig plane. Since most of the obstacles appear vertically relative to the world coordinate system, Labayrade's plane definition will encounter errors due to the stereo rig's pitch angle.

In this paper, we define all the planes with respect to the WCS as shown in Fig.4. In a typical driving environment, horizontal planes can be generally referred to the ground surface nearby, while slopes can be treated as the oblique planes. The rear panel of the vehicle ahead will show a partial vertical plane.

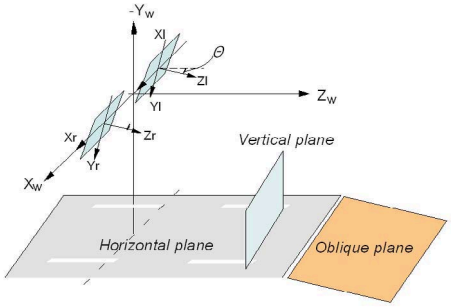

Fig.4. Three basic planes in WCS

A. Horizontal planes

Horizontal planes can be simply described as (10) in the WCS:

$$Y_w = h \quad (10)$$

Combining with equations (7) and (8), we can deduce the following linear equation with respect to the left image:

$$\frac{h}{b}\Delta = f \sin\theta + V \cos\theta \quad (11)$$

Equation (11) shows that horizontal planes in the WCS will be projected as straight lines in the V-disparity domain.

B. Vertical planes

Vertical planes can be described as (12) in the WCS:

$$Z_w = p \quad (12)$$

Combining with equations (7) and (8), we can deduce the following linear equation with respect to the left image:

$$\frac{p}{b}\Delta = f \cos\theta - V \sin\theta \quad (13)$$

It shows that vertical planes in the WCS will be projected as near vertical straight lines in the V-disparity domain. When the pitch angle θ is small enough, equation (13) will be simplified as equation (14), which corresponds to the stereo principle equation (1).

$$\Delta \approx \frac{b}{p} f \cos\theta \quad (14)$$

C. Oblique planes

Oblique planes can be described as (15) in the WCS:

$$Z_w = \alpha Y_w + \beta \quad (15)$$

Combining with equations (7) and (8), we can deduce the following linear equation with respect to the left image:

$$\frac{\beta}{b}\Delta = f(\cos\theta - \alpha \sin\theta) - V(\sin\theta + \alpha \cos\theta) \quad (16)$$

It shows that vertical planes in the WCS will also be projected as straight lines in the V-disparity domain.

D. Other planes

Besides the three types of planes described above, many other surface planes exist in the general driving environment. Examples include vehicle side surfaces, guardrails, roadside or overpass structures, etc. Fig. 5 shows the typical geometrical models of these planes.

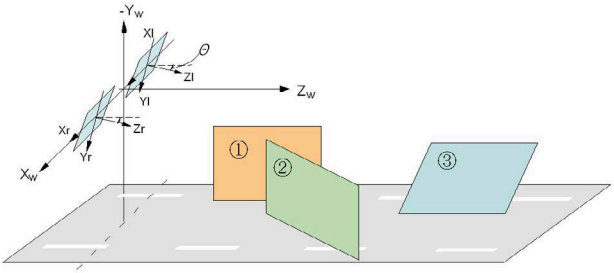

Fig.5. Other planes in WCS

The side surfaces of vehicles and of most roadside structures are parallel to the Y-Z plane in the WCS (marked as ① in Fig.5), which can be described as:

$$X_w = r \quad (17)$$

Combining with equations (7) and (8), we can deduce the following linear equation with respect to the left image:

$$\frac{2r+b}{2b}\Delta = U \tag{18}$$

Equation (18) shows that in the U-disparity domain, all side surfaces parallel to the Y-Z plane in the WCS will be projected as straight lines passing through the optical origin.

Cutting-in vehicles and some roadside structures may show the side surface planes marked as ② in Fig.5. These can be described as follows in the WCS:

$$Z_w = \rho X_w + \tau \tag{19}$$

Combining with equations (7) and (8), we can deduce the following linear equation with respect to the left image:

$$\rho U + V\sin\theta + \frac{2\tau - \rho b}{2b}\Delta = f\cos\theta \tag{20}$$

When the pitch angle θ is small enough, equation (20) can be simplified as:

$$\rho U = \frac{\rho b - 2\tau}{2b}\Delta + f \tag{21}$$

Equation (21) describes the fact that oblique side surfaces can be approximately treated as straight lines in the U-disparity domain when pitch angle is small.

There is still a special case for side surfaces that needs to be considered when the stereo rig's roll angle around the Z-axis is not zero. In this situation, the epipolar lines are not parallel to the ground surface and all vertical side surfaces will be oblique with respect to Z-axis in the WCS as shown in Fig.5 (marked ③). The geometric model for these planes in the WCS is:

$$Y_w = \gamma X_w + \delta \tag{22}$$

Combining with equations (7) and (8), the following linear equation holds with respect to the left image:

$$\gamma U + V\cos\theta + \frac{2\delta - \gamma b}{2b}\Delta = f\sin\theta \tag{23}$$

3.4. U-V-disparity domain construction and 3D surface extraction

Once the disparity map is generated by the matching between left and right images, all pixels on the disparity map $\Delta(u,v)$ based on left image will be converted to the new disparity map $\Delta(U,V)$ with respect to the optical centre, where $U = u - u_0$ and $V = v - v_0$. The domain of U-disparity and V-disparity will then be built by accumulating the pixels with the same (U,Δ) or (V,Δ) values.

From equation (11), (13), (16) and (18), extracting straight lines from the U-disparity domain and V-disparity domain leads to extract most kind of 3D surfaces in WCS. If the constraint of small pitch angle is satisfied, equation (14) and (21) supplement the 3D surface extraction result.

Any robust algorithms for 2D line extraction can be used like Hough transformation, geometric Hashing or other voting algorithms.

4. Implementation and Experiments

4.1. A fast stereovision module

We have implemented a fast stereo module based on SSDA block matching algorithm. By careful management of cache memory and SSE technology on Pentium processor, our module can achieve real-time processing speed for dense disparity computation on a 320 by 240 image with the maximum disparity of 32 pixels. Table 1 indicates the performance of our stereovision module.

Fig.6 show the disparity map result followed by a pseudo color LUT, where warmer color shows a bigger value of disparity. The grey mask area indicate "don't care" region.

Table 1. Performance by image size and search range (CPU: PentiumIV 2.26GHz)

Maximum disparity (pixel)	Image Size (pixel)	Processing time (ms)
32	160*120	5.99
16	320*240	13.91
32	320*240	24.95
32	640*480	99.80

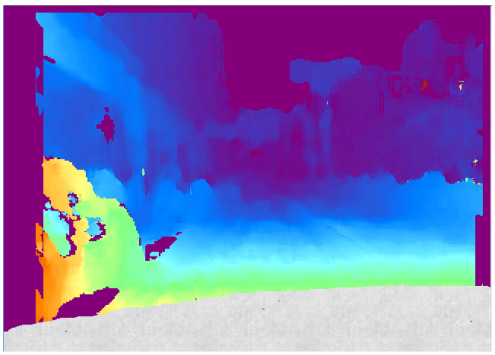

Fig.6. Disparity map of Fig.1

4.2. Synthetic stereo image test on "U-V-disparity"

Fig.7 (a) and (b) are well-used synthetic stereo test image pair, and the ground truth disparity map is shown in Fig.7(c). Fig.8 shows the calculated U-disparity and V-disparity domain. Pixels will not be counted if its value is lower than a predefined threshold. The final line extraction results by Hough transformation are shown in Fig.9.

Finding correspondence between the 3D surface planes with the line extraction result becomes less difficult with

our previous conclusion in Section 3.3. Ground surface plane is projected to the V-disparity domain as straight line (marked as ②) with a slope angle. Ceiling surface is also projected as straight line (marked as ⑪), which intersects at the same point in V-axis with ground surface projection in V-disparity domain, because it is parallel to the ground surface in WCS.

Sidewall surfaces are clearly corresponding to the straight lines (marked as ⑥⑦) in U-disparity domain towards to the optical center. Vertical obstacles (marked as ⑨) and intersection walls (marked as ③④⑧⑩) can be extract from both U-disparity and V-disparity domain since pitch angle is small, as described in Section 3.3. Since curved surface will not be discussed in this paper, only approximated straight line segments (marked as ① ⑤) are extracted, which are corresponding to the ball and cone respectively.

(a) (b) (c)
Fig.7. Synthetic test stereo images and disparity map

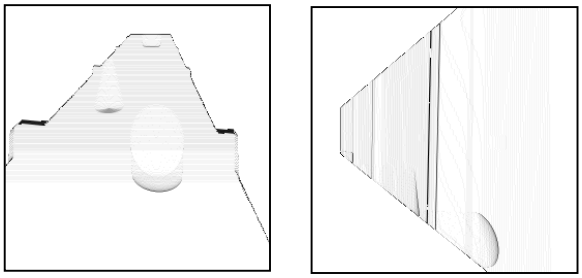

(a) U-disparity domain (b) V-disparity domain
Fig.8. Calculated U-V-disparity

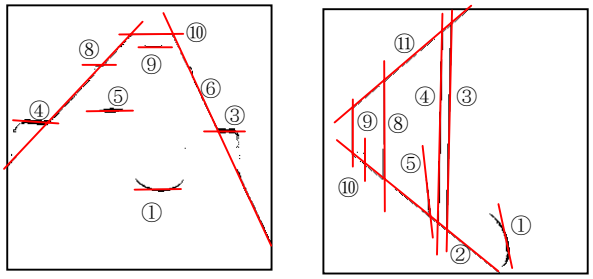

Fig.9. Line extraction result on U-V-disparity

In order to reconstruct the 3D scene with the extracted surface planes, all pixels in U-V-disparity domain that contribute to the extracted lines are projected back to the disparity map, with the label of 2D lines. Pixels are grouped with the same label and surrounded by a polygon as shown in Fig.10. In order to accelerate the conversion and clustering process, three look-up tables (LUT) are generated based on disparity map $\Delta(U,V)$, label map in U-disparity domain $L(U,\Delta)$ and label map in V-disparity domain $L(V,\Delta)$.

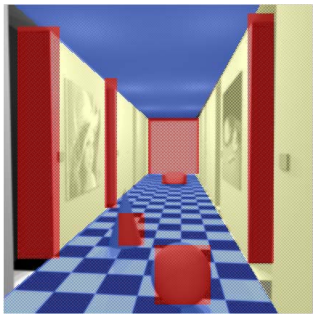

Fig.10. 3D scene reconstruction result

4.2. Real driving environment experiments

Two synchronized TELI CS8550i progressive cameras are mounted on the stereo rig with the baseline of 42mm. In order to have a wider FOV, we chose the camera lens with focal of 4.2mm. Calibration and pre-processing have undistorted and rectified the stereo images, and kept epipolar lines in horizontal.

Fig.11 shows some sample images and calculated disparity maps. Calculation results of U-V-disparity domain are shown in Fig.12, extracted line segments are marked in red.

In the first test image, ground surface planes are projected to the V-disparity domain as straight line (marked as ①) with a slope angle. Vehicles rear panel can be extracted from both U-disparity and V-disparity domain as straight lines (marked as ②③④⑤) since pitch angle is small. It is interesting to see that the passenger car ahead in the same lane has the similar disparity and vertical coordinates with the truck nearby, using only V-disparity domain cannot separate the two vehicles properly. By checking the corresponding lines in U-disparity domain, it is easy to distinguish which line belongs to the rear panel of passenger car, which line belongs to the side surface and rear panel of the truck.

Ground surface planes are also clearly projected to the V-disparity domain as straight line (marked as ①) in the second test image. Since the building and the light truck on the left showed oblique side surfaces, with respect to our previous conclusion in Section 3.3, they can be

approximately treated as straight lines in the U-disparity domain when pitch angle is small. Extraction result (marked as ②③) verified our conclusion. The truck crossing the intersection showed side surface as vertical plane in WCS, and its projection in U-disparity and V-disparity domain was extracted as a vertical straight line (marked as ④). Pole and guardrail are also properly extracted from U-V-disparity domain (marked as ⑤⑥).

In order to properly match the 3D surface planes with the extracted 2D lines, all pixels in U-V-disparity domain that contribute to the extracted lines as well as pixels surround them are projected back to the disparity map, with the label of 2D lines. Pixels are grouped with the same label and surrounded by a polygon like shown in Fig.12. Red regions belong to the vertical surface planes, blue regions belong to the ground surface and yellow regions belong to the side surface planes. The result perfectly matches with human's analysis and verifies the effectiveness of the proposed method.

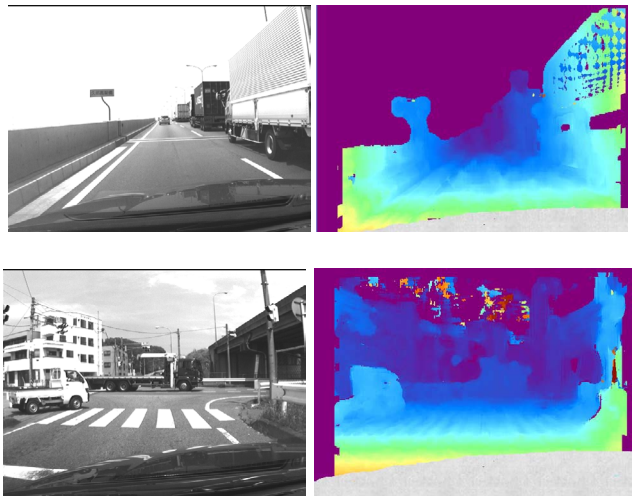

Fig.10. Real driving scene images and disparity maps

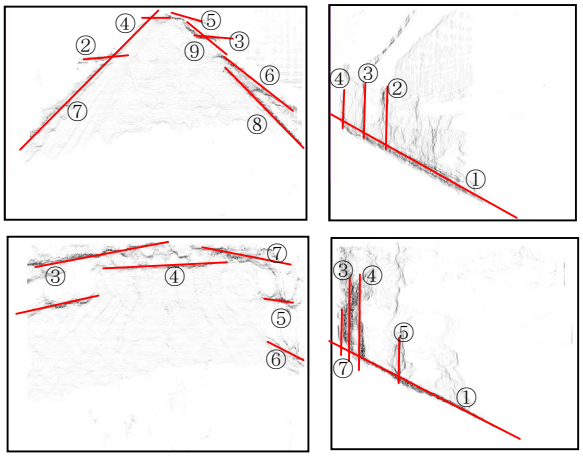

(a) U-disparity domain (b) V-disparity domain

Fig.11. Calculated U-V-disparity and line extraction result

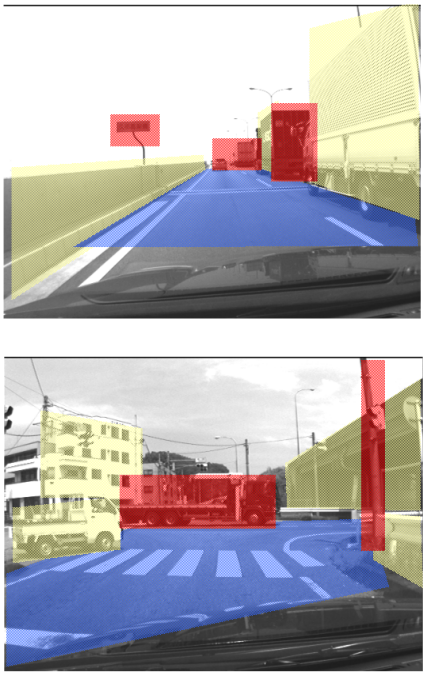

Fig.12. Reconstructed 3D driving environment

5. Conclusions

We have proposed a complete study of U-V-disparity concept for driving environment analysis. A stereovision based sensing system provides an effective supplement to radar-based road scene analysis with its much wider field of view and more accurate lateral information. This paper presents an efficient solution using a stereovision based road scene analysis algorithm that employs the "U-V-disparity" concept. This concept is used to classify a 3D road scene into relative surface planes and characterize the features of road pavement surfaces, roadside structures and obstacles. Real-time implementation of the disparity map calculation and the "U-V-disparity" classification is also presented.

References

[1] Q.T. Luong, J. Weber, D. Koller and J. Malik, "An integrated stereo-based approach to automatic vehicle guidance," *Fifth International Conference on Computer Vision (ICCV '95)*, Cambridge, Mass, pp. 52-57, June 1995

[2] Changming Sun, "Fast Stereo Matching Using Rectangular Subregioning and 3D Maximum-Surface Techniques", *International Journal of Computer Vision*, vol.47, No.1/2/3, pp.99-117, May 2002

[3] Yoshiki Ninomiya, Takeo Kato, Yoshiko Kojima, "Sensor Fusion for Road Environment Recognition", *Review of Toyota CRDL*, vol.36, No.3, pp.27-34, Sep. 2001

[4] W. Enkelmann, "Obstacle detection by evaluation of optical flow fields form image sequence," *Image and Vision Computing*,

pp. 160-168, 1991
[5] M.H.Young, T.H. Hong and A.Yang, “Obstacle detection for a vehicle using optical flow,” *SAE Intelligent Vehicle*. IEEE, 1992
[6] R. Nelson and J. Aloimonos, “Using flow field divergence for obstacle avoidance: towards qualitative vision,” *Proc. Of International Conference on Compute Vision*, pp.188-196, 1988
[7] U. Hofmann, A. Rieder and E.D. Dickmanns, “Radar and Vision Data Fusion for Hybrid Adaptive Cruise Control on Highways”, *ICVS 2001*, pages 125-138, 2001
[8] M.Bertozzi, A.Broggi, A.Fascioli, S.Nichele, “Stereo Vision based Vehicle Detection,” *Proceedings of IEEE Intelligent Vehicle Symposium*, Oct. 2000
[9] A.Talukder, R. Manduchi, A. Rankin, L. Matthies, “Fast and Reliable Obstacle Detection and Segmentation for Cross-country Navigation”, *Proceedings of IEEE Intelligent Vehicle Symposium*, Versailles, France, 2002
[10] Raphael Labayrade, Didier Aubert, Jean-Philippe Tarel, “Real Time Obstacle Detection in Stereovision on Non Flat Road Geometry Through "V-disparity" Representation", *Proceedings of IEEE Intelligent Vehicle Symposium*, June 2002
[11] A. Sole, O. Mano, G.P.Stein, H.Kumon, Y.Tamatsu, A. Shashua, “Solid or not solid: Vision for radar target validation,” *Proceedings of IEEE Intelligent Vehicle Symposium*, June 2004